Proton Abstraction Mediates Interactions Between the Super Photobase **FR0-SB** and Surrounding Alcohol Solvent

Jurick Lahiri¹, Mehdi Moemeni¹, Jessica Kline¹, Babak Borhan^{1,*}, Ilias Magoulas¹, Stephen H. Yuwono¹, Piotr Piecuch^{1,2,*}, James E. Jackson^{1,*}, Marcos Dantus^{1,2,*} and G. J. Blanchard^{1,*}

Abstract

We report on the motional and proton transfer dynamics of the super photobase FR0-SB in the series of normal alcohols C1 (methanol) through C8 (*n*-octanol) and ethylene glycol. Steady-state and time-resolved fluorescence data reveal that the proton abstraction dynamics of excited FR0-SB depend on the identity of the solvent and that the transfer of the proton from solvent to FR0-SB*, forming FR0-HSB^{+*}, fundamentally alters the nature of interactions between the excited molecule and its surroundings. In its unprotonated state, solvent interactions with FR0-SB* are consistent with slip limit behavior, and in its protonated form, intermolecular interactions are consistent with a much stronger interaction of FR0-HSB^{+*} with the deprotonated solvent RO⁻. We understand the excited state population dynamics in the context of a kinetic model involving a transition state wherein FR0-HSB^{+*} is still bound to the negatively charged alkoxide, prior to solvation of the two charged species. Data acquired in ethylene glycol confirm the hypothesis that the rotational diffusion dynamics of FR0-SB* are largely mediated by solvent viscosity while proton transfer dynamics are mediated by the lifetime of the transition state. Taken collectively, our results demonstrate that FR0-SB* extracts solvent protons efficiently and in a predictable

¹ Department of Chemistry, Michigan State University, East Lansing, MI 48824, USA

² Department of Physics and Astronomy, Michigan State University, East Lansing, MI 48824, USA

^{*} Corresponding authors: BB email: babak@chemistry.msu.edu, tel.: +1-517-353-0501; PP email: piecuch@chemistry.msu.edu, tel.: +1-517-353-1151; JEJ email: jackson@chemistry.msu.edu, tel.: +1-517-353-0504; MD email: dantus@chemistry.msu.edu, tel.: +1-517-353-1191; GJB email: blanchard@chemistry.msu.edu, tel.: +1-517-353-1105.

manner, consistent with a *ca*. three-fold increase in dipole moment upon photoexcitation as determined by *ab initio* calculations based on the equation-of-motion coupled-cluster theory.

Introduction

The ability to activate chemical reagents to perform spatially and temporally localized reactions affords many opportunities in areas ranging from materials science to the modulation of intracellular phenomena. Central to such precision chemistry is the use of photoinitiated reactive species, with the most common type being super photoacids.¹⁻² Such species exhibit a large negative change in the pK_a of an acidic proton upon excitation, typically to the first excited electronic state. The reactive counterpart to a super photoacid is a super photobase. Presently there are two known examples of super photobases, 5-methoxyquinoline (5MQ),³ and FR0-SB (Fig. 1), a compound that exhibits a large negative change in pK_b of an imine upon excitation to its S₁ state.⁴ While the unique properties of this molecule show much promise for future work on localized photoinitiated chemical reactions, a detailed understanding of the factors responsible for this behavior and of the dynamics of solvent interactions and proton abstraction remain to be elucidated. Among the reasons for the need for this information is to design other photobases with tailored properties (e.g., $\Delta pK_a = pK_a^* - pK_a$) and to understand the structural and electronic factors that control the photobase lifetime, because it is this property that determines the diffusionmediated resolution of any photoinitiated reaction using such reagents. We report here on the lifetime and solvent-interaction dynamics for FR0-SB in a series of normal alcohols and ethylene glycol.

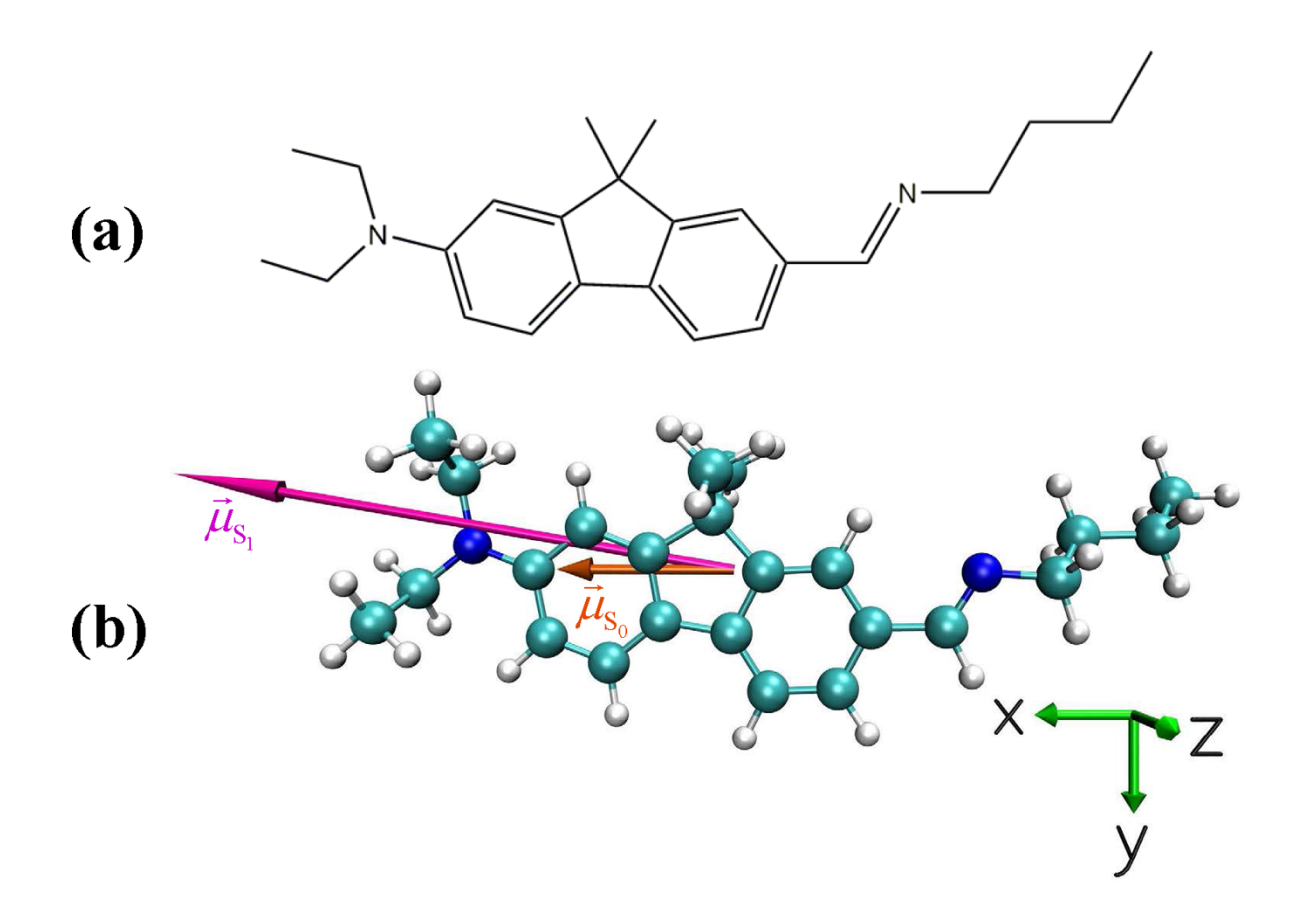


Fig. 1: (a) **FR0**-SB super photobase. (b) The structure of the isolated **FR0**-SB molecule in its ground electronic (S₀) state and the dipole moments characterizing the S₀ (shorter orange vector $\vec{\mu}_{S_0}$) and electronically excited S₁ (longer magenta vector $\vec{\mu}_{S_1}$) states, as calculated in this work.

For any condensed phase chemical reaction, the interactions of the reactant(s) with their immediate environments typically play a critical role in the rate and specificity of the reaction. For **FR0**-SB, photoexcitation leads to proton abstraction from its local environment in protic solvents. There are multiple consequences to this abstraction event, ranging from the generation of another strong base, *i.e.*, RO⁻, to structural and electronic changes in the photobase that occur due to the addition of a proton. These excitation-induced changes can be characterized using time-resolved spectroscopy and we provide a detailed discussion of results from such measurements. First,

however, we consider the steady-state spectroscopic properties of **FR0**-SB and how these data can be explained in the context of a simple kinetic model. With this understanding in place, we can interpret the time-resolved fluorescence data in the context of proton transfer processes. These results indicate that the addition of a proton to **FR0**-SB* alters the nature of its interactions with its immediate surroundings in a pronounced manner, pointing to the importance of solvent-solute interactions in understanding condensed phase dynamics and providing insight into molecular design strategies to gain direct control over proton transfer processes.

Experimental Section

Materials. Anhydrous alcohols from methanol to *n*-octanol and ethylene glycol were obtained from MilliporeSigma in their highest purity grade available and used without further purification.

The compound **FR0**-SB was synthesized from **FR0** and *n*-butyl amine as described below. 7-(diethylamino)-9,9-dimethyl-9*H*-fluorene-2-carbaldehyde (FR0):

The synthesis of **FR0** followed the procedure reported previously, and is described briefly here.⁴ The synthesis commenced with the bromination of fluorene at C2 with N-bromosuccinimide (NBS). The gem-dimethyl group at C9 was installed with the reaction of the brominated fluorene with iodomethane in the presence of NaOH. Nitration with fuming nitric acid yielded 2-bromo-9,9-dimethyl-7-nitro-9*H*-fluorene, which was subsequently reduced to the corresponding amine with iron powder suspended in an aqueous ammonium chloride solution. The resulting product was heated with ethyl iodide and potassium carbonate to introduce the diethyl substituents on the amine. **FR0** was obtained upon formylation of the resultant metal/halogen exchanged intermediate (exchange promoted by the addition of *n*-butyl lithium) as a yellow solid.

FR0-SB:

FR0 (10.5 mg, 35.8 μmol) was dissolved in ethanol (3.0 mL), and *n*-butylamine (100 μL, 28.2 equiv.) was added. The resulting solution was stirred at room temperature for 2 h, after which the solvent and excess *n*-butylamine were removed under reduced pressure, affording a light yellow solid (**FR0**-SB) as an analytically pure product (12.5 mg, 99%). ¹H NMR (CDCl₃, 500 MHz), δ (ppm): 8.30 (s, 1H), 7.83 (d, J = 1.3 Hz, 1H), 7.61 – 7.51 (m, 3H), 6.74 – 6.65 (m, 2H), 3.67 – 3.60 (m, 2H), 3.45 (q, J = 7.1 Hz, 4H), 1.72 (p, J = 7.2 Hz, 2H), 1.50 (s, 6H), 1.47 – 1.39 (m, 2H), 1.23 (t, J = 7.0 Hz, 6H), 0.98 (t, J = 7.4 Hz, 3H); ¹³C NMR (CDCl₃, 125 MHz), δ (ppm): 161.52, 156.42, 153.14, 148.22, 142.73, 133.14, 128.59, 126.33, 121.49, 120.85, 118.09, 110.74, 105.49, 61.64, 46.70, 44.70, 33.22, 27.43, 20.52, 13.97, 12.64. ESI-MS: (calc.) (m/z) calc'd. for $C_{24}H_{33}N_2$ [M+H]⁺ 349.2644, found 349.2643.

Steady-state absorbance and emission spectroscopy. UV-visible absorption spectra were recorded using a Shimadzu UV-2600 UV-vis spectrometer. Spectral resolution was 1 nm for all measurements reported here. The concentration of the samples was 10 μ M in all the solvents. Using a 1 cm cuvette, the OD of the samples at the absorbance maximum was 0.82 ($\epsilon_{max} \sim 81,500$ M⁻¹ cm⁻¹). While this OD is somewhat higher than usual, we acquired steady state and time-resolved data for **FR0**-SB in several solvents at OD 0.1 and obtained results that are identical to those acquired using the 10 μ m samples. These data are contained in Table S1. All absorbance and emission data were acquired at room temperature (20 ± 1°C). Fluorescence spectra for the dye while dissolved in the solvents were obtained using a Hitachi FL-4500 fluorescence spectrometer with excitation at maximum absorption. Spectral resolution was 1 nm for all measurements reported here.

Time-resolved fluorescence measurements. The time-correlated single photon counting (TCSPC) instrument used in this work has been described elsewhere⁵ in detail and we highlight its salient features here. The light source for this instrument is a passively mode-locked Nd:YVO₄ laser (Spectra Physics Vanguard) that produces 13 ps pulses at 1064 nm with 80 MHz repetition rate. The second and third harmonic outputs of this laser provide 2.5 W average power at 532 nm and 355 nm, respectively, with nominally the same 13 ps pulsewidth. The second harmonic output of this laser was used to excite a synchronously pumped cavity-dumped dye laser (Coherent 701-3) operating at 700 nm (LDS 698 laser dye, Exciton). The fundamental output of the dye laser was frequency-doubled using a Type I SHG crystal (LiIO₃, 1 mm) to produce 350 nm excitation pulses (ca. 5 ps pulse, 120 ns inter-pulse spacing) to excite the **FR0**-SB samples. Average power at the sample was 0.5 mW or less for all measurements and the sample temperature was maintained at room temperature (20 ± 1 °C). A portion of the 700 nm pulse-train was sent to a reference photodiode (B&H). Sample fluorescence was collected using a 40x reflecting microscope objective (Ealing) and sent to a polarization-selective beamsplitter (Newport). Each polarized emission component was polarization-scrambled and sent through a subtractive double monochromator (CVI Digikrom CM112) to a microchannel plate photomultiplier (Hamamatsu RG3809). The output of each detection channel was sent to one channel of a TCSPC system (B&H Simple Tau 152) and to a personal computer. Data were acquired and stored using software written in-house using National Instruments LabVIEW®. For each individual data set, the maximum signal channel contained at least 1500 counts, and at least three individual data sets were acquired for FR0-SB in each solvent studied.

The experimental fluorescence lifetime $(I_{\parallel}(t)+2I_{\perp}(t))$ and anisotropy decay functions, R(t), were constructed from raw polarized fluorescence transients that were tail-matched at times long

relative to the anisotropy decay time. The resulting experimental anisotropy decay function data were fitted to either one- or two-component exponential decays using Microcal Origin 9.0 software. The instrumental response function for the TCSPC instrument (ca. 40 ps) is sufficiently short that it was not necessary to deconvolute it from the fluorescence transients. We provide example data and fits in Figs. S1 – S4.

Computational Details

The purpose of the electronic structure calculations reported in this work was to determine some of the key properties of the ground (S₀) and low-lying excited singlet electronic (S_n, n > 0) states of the isolated **FR0**-SB molecule, which are relevant to this work, including the ground-state geometry, the excitation energies and oscillator strengths characterizing the vertical S₀ \rightarrow S_n transitions, and the electronic dipole moments of the calculated states. With the exception of the molecular geometry, which was optimized using the Kohn-Sham formulation⁶ of the density functional theory (DFT),⁷ all of the characteristics of the calculated electronic states were obtained using high-level *ab initio* methods of quantum chemistry based on the coupled-cluster (CC) theory⁸ and its equation-of-motion (EOM) extension⁹ to excited states.

Given the relatively large size of the **FR0**-SB molecule, which consists of 58 atoms and 190 electrons, in order to use the CC and EOMCC methods as fully as possible, and to make sure that the higher-order many-electron correlation effects beyond the basic EOMCC singles and doubles (EOMCCSD)⁹ level are properly accounted for, we used the following composite approach to determine the vertical excitation energies corresponding to the $S_0 \rightarrow S_n$ transitions:

$$\omega_n^{(\text{EOMCC})} = \omega_n^{(\text{EOMCCSD/6-31+G*})} + \left[\omega_n^{(\delta\text{-CR-EOMCC(2,3)/6-31G})} - \omega_n^{(\text{EOMCCSD/6-31G})}\right]. \tag{1}$$

The first term on the right-hand side of Eq. (1) denotes the vertical excitation energy obtained in the EOMCCSD calculations using the 6-31+G* basis set, ¹⁰⁻¹² which was the largest basis set we

could afford in such computations. The next two terms on the right-hand side of Eq. (1), which represent the difference between the δ -CR-EOMCC(2,3) and EOMCCSD vertical excitation energies obtained using a smaller 6-31G basis, 10 correct the EOMCCSD/6-31+G* results for the higher-order many-electron correlation effects due to triple excitations. We recall that the δ -CR-EOMCC(2,3) approach¹³ is a rigorously size-intensive modification of the completely renormalized EOMCC methodology, abbreviated as CR-EOMCC(2,3), 14-16 which provides a recipe how to correct EOMCCSD energies for the leading triple excitations in a robust manner and which is an extension of the CR-CC(2,3) triples correction 14-15, 17-18 to CCSD 19 to excited electronic states. For example, in a report²⁰ where about 200 excited states of 28 organic molecules were examined using a variety of EOMCC methods, it was shown that one needs triples corrections, such as those of the δ -CR-EOMCC(2,3) approach, on top of EOMCCSD to obtain a quantitative description (errors reduced to a $\sim 0.1-0.2$ eV level). The size intensivity of the EOMCCSD and δ -CR-EOMCC(2,3) excitation energies entering our composite computational protocol defined by Eq. (1), combined with the size extensivity of the underlying CCSD and CR-CC(2,3) approaches, is important too, since without reinforcing these formal theory features one risks losing accuracy with growing molecular size.

The CCSD/6-31+G* and EOMCCSD/6-31+G* calculations were also used to determine the dipole moments in the ground and excited states and the oscillator strengths characterizing the vertical $S_0 \to S_n$ (in general, $S_m \to S_n$) transitions. As usual, this was done by solving both the right and the left EOMCCSD eigenvalue problems and constructing the relevant one-electron reduced density and transition density matrices.^{9,21} While triples corrections, such as those of CR-CC(2,3) and δ -CR-EOMCC(2,3), are important to improve the energetics, the description of one-electron properties, such as dipole moments and oscillator strengths characterizing one-electron

transitions examined in this study, by the CCSD and EOMCCSD approaches is generally quite accurate.

All single-point CC and EOMCC calculations reported in this work relied on the ground-state geometry of FR0-SB, which we optimized using the analytic gradients of the CAMB3LYP DFT approach²² employing the 6-31+G* basis set. We chose the CAMB3LYP functional because the extension of this functional to excited states using the time-dependent (TD) DFT formalism²³ provided vertical excitation energies closest to those obtained with EOMCC. Furthermore, the ground-state geometry of the FR0-SB molecule resulting from the CAMB3LYP/6-31+G* calculations turned out to be virtually identical (to within 0.004 Å on average and not exceeding 0.02 Å for the bond lengths) to that obtained with the second-order Møller-Plesset perturbation theory (MP2) approach using the same basis.

All of the electronic structure calculations for the **FR0**-SB molecule reported in this study, including the CAMB3LYP and MP2 geometry optimizations and the CC/EOMCC single-point calculations, were performed using the GAMESS package.²⁴ The relevant CCSD, EOMCCSD, and δ-CR-EOMCC(2,3) computations using the restricted Hartree-Fock (RHF) determinant as a reference and the corresponding left-eigenstate CCSD and EOMCCSD calculations, which were needed to determine the triples corrections of δ-CR-EOMCC(2,3) and the one-electron properties of interest, including the dipole moments and oscillator strengths, were carried out using the CC/EOMCC routines developed by the Piecuch group,^{14, 16-18, 21, 25-26} which form part of the GAMESS code. In all of the post-RHF calculations, the core orbitals associated with the 1s shells of C and N atoms were kept frozen, *i.e.*, we correlated 138 electrons. In the calculations employing the 6-31+G* basis set, we used spherical d-type polarization functions. The visualization of the

optimized structure of **FR0**-SB in its ground electronic state shown in Fig. 1 (b) was accomplished using VMD software.²⁷

Results and Discussion

The central issue of concern is how the excited state of the super photobase **FR0**-SB interacts with the surrounding solvent before and after photoexcitation. We initiate our study by surveying the steady-state fluorescence spectra of **FR0**-SB in normal alcohols, which show two prominent emission bands. One band is associated with the (initially) unprotonated form, **FR0**-SB* (*ca.* 460 nm), and the other is associated with the protonated form, **FR0**-HSB^{+*} (*ca.* 630 nm). As can be seen from the spectra (Fig. 2), the relative intensities of the two emission bands depend on the solvent medium.

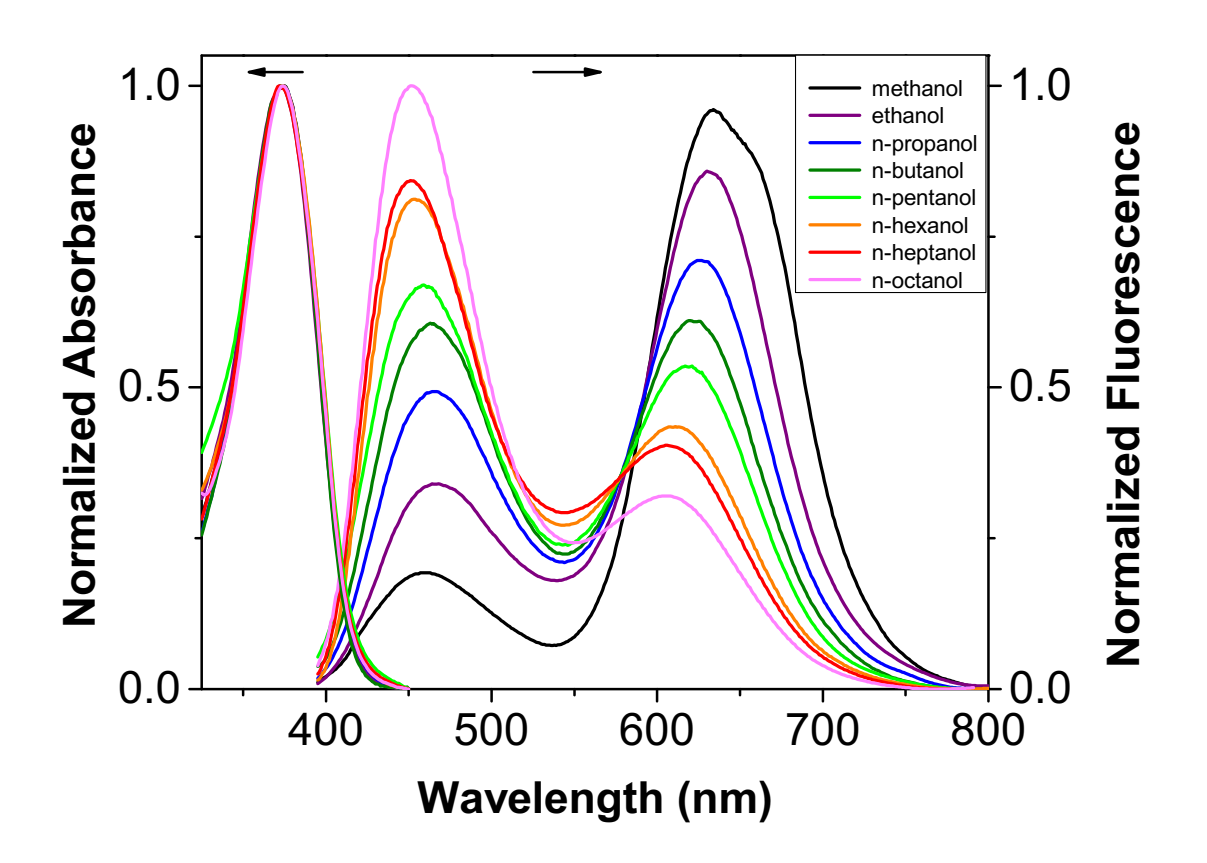


Fig. 2: The normalized absorption (left) and fluorescence (right) spectra of **FR0**-SB in linear alcohols from methanol to *n*-octanol. Absorbance spectra are normalized to a maximum of 1.0 and integrated emission band areas are normalized for area.

In order to examine the interactions between the super photobase and its immediate environment, we measure the rotational diffusion dynamics of both **FR0**-SB* and **FR0**-HSB⁺*. For such measurements, we acquired fluorescence transients for polarizations parallel and perpendicular to the excitation polarization in each solvent ($I_{||}(t)$) and $I_{\perp}(t)$, respectively). The transients are combined to produce the induced orientational anisotropy decay function,

$$R(t) = \frac{I_{\parallel}(t) - I_{\perp}(t)}{I_{\parallel}(t) + 2I_{\perp}(t)}.$$
 (2)

The chemical and physical information of interest lies in the functional form and decay time constant(s) of R(t), and there is a well-established theoretical framework in place for the interpretation of these data.²⁸⁻³¹ The relationship between the anisotropy decay function and the Cartesian components of the rotational diffusion constant (D_i , i = x,y,z) have been described by Chuang and Eisenthal.²⁸ For the experimental conditions of relevance here, the transition dipole moment between the ground state and the first excited singlet state lies approximately along the long molecular axis (x), which is taken to be unique relative to the short molecular axes (y, z) (see Fig. 1 (b)). Such motion is described in the context of a prolate rotor ($D_x \neq D_y = D_z$), and R(t) decays as a single exponential. The recovered anisotropy decay time constant is inversely related to D_z .

Under these experimental conditions, the rotational diffusion decay time constant is related to chromophore and system properties through the modified Debye–Stokes–Einstein (DSE) equation, ²⁹⁻³¹

$$\tau_{\rm OR} = \frac{1}{6D_z} = \frac{\eta V f}{k_{\rm B} T S},\tag{3}$$

where $\tau_{\rm OR}$ is the decay time constant of R(t), η is the (bulk) solvent viscosity, V is the hydrodynamic volume of the rotating entity, calculated using the method of van der Waals increments,³² f is a frictional interaction term that describes the boundary condition between solvent and solute, 30 $k_{\rm B}T$ is a thermal energy term and S is a shape factor related to the ellipsoidal shape of the rotating molecule, calculated using Perrin's equations.³¹ Using molecular mechanics we estimated the major axis length of FR0-SB to be 18.2 Å and the minor axis to be 6.2 Å, yielding a hydrodynamic volume of 363 Å³, in agreement with the estimate from the method of van der Waals increments.³² From the ratio of the axes, $\rho = 0.34$, and using Perrin's equation for a prolate ellipsoid, we recover S = 0.43. The choice of a prolate ellipsoid was based on the observed single exponential anisotropy decay in all cases (vide infra). For strong intermolecular interactions, f is set to 1, the so-called stick limit. For conditions where the interactions between solvent and chromophore are less strong, f can range from 0 to ≤ 1 , depending on the value of S. For a prolate rotor with S = 0.43, $f_{slip} = 0.44$. This is the so-called slip limit. In our consideration of solventchromophore interactions, we do not attempt to correct for changes in S because any such correction would lead to only small changes in the model results and there is no experimental means of evaluating any such change.

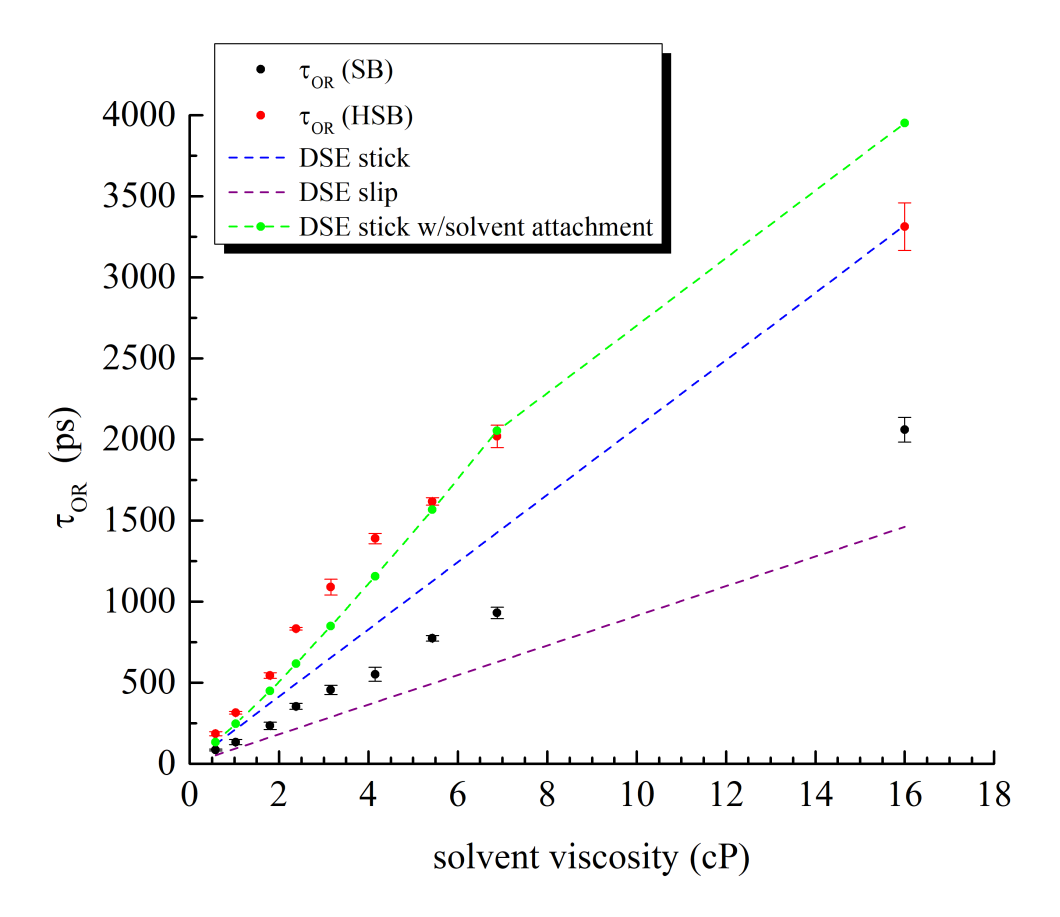


Fig. 3: Reorientation times of **FR0**-SB* and **FR0**-HSB^{+*} in the primary *n*-alcohols, methanol through 1-octanol, and ethylene glycol plotted *vs.* solvent viscosity. The purple and blue dashed lines indicate the slip and stick limit from the modified DSE equation, Eq. (3), respectively. The green points represent the result of solvent "attachment" to the chromophore.

Despite the fact that the modified DSE model assumes the solvent to be a continuum, it has proven to be a relatively accurate predictor of rotational diffusion behavior. For the experiments reported here, the rotational diffusion dynamics for the unprotonated **FR0**-SB* system are measured at 450 nm, and the rotational diffusion dynamics of the protonated **FR0**-HSB** species are measured at 650 nm. The normalization for the total excited state population (the denominator

in Eq. (2)) ensures that the fluorescence decay or the fluorescence rise in the case of the protonated species, do not distort the motional information content of R(t). We show in Fig. 3 the experimental reorientation times for **FR0**-SB* and **FR0**-HSB^{+*} as a function of solvent viscosity, along with the predictions of the modified DSE model in both the stick and slip limits. We find that the anisotropy decay time constant varies linearly with solvent viscosity for both species, however, the slope of the dependence is different by a factor of slightly more than two (291 ps/cP for **FR0**-HSB^{+*} vs. 134 ps/cP for **FR0**-SB*). We consider this difference in more detail next.

As can be seen from the lines in Fig. 3 calculated using the modified DSE model in the stick and slip limits, the reorientation behavior of FR0-HSB^{+*} appears to be slower than the stick limit, while that of FR0-SB* is intermediate between stick and slip limits. Following proton transfer, FR0-HSB^{+*} is positively charged and there is a negatively charged RO⁻ species nearby. The difference in behavior between FR0-SB* and FR0-HSB^{+*} is consistent with the difference predicted by the stick and slip limits. We believe this to be largely fortuitous. The modified DSE model in either limit does not account for intermolecular interactions between chromophore and solvent that are central to the data we report here.

Despite the apparent appeal of the stick and slip limit predictions, it is important to also consider the process that is relevant to our observations. Specifically, the process under consideration is a proton transfer event from the ROH solvent to the **FR0**-SB* chromophore. The products of this process are described as RO⁻ and **FR0**-HSB^{+*}, with the necessary involvement of a transition state (see Fig. 4). This representation has been made previously for **FR0**-SB*, where

$$SB^* \cdots H \cdot OR \rightleftharpoons SB^* \cdots H \cdots OR \rightleftharpoons SB^* - H \cdots OR$$

Fig. 4: Schematic of proton exchange between SB* and solvent.

the excited state proton transfer reaction coordinate is indicated as having a local minimum intermediate between FR0-SB* and FR0-HSB^{+*}. The open issue is the timescale of the transition from unprotonated to protonated form (Fig. 4) and the ability to distinguish a "shared" proton from a contact ion pair (FR0-HSB^{+*} - OR) based on the data reported here. In fact, the reorientation data cannot provide explicit information on the nature of the solvent-solute pair. If the solvent-(excited) solute complex (Fig. 4) is stable on a time-scale similar to the rotational time of the chromophore, the complex, including both the chromophore and solvent molecule hydrodynamic volume, would contribute to the hydrodynamic volume of the rotating species. Such a solventsolute complex can be modeled by $V = V_{FR0-SB^*} + V_{ROH}$, which is presented as the green dots and connecting line in Fig. 3. In such a system it is expected that for sufficiently slow reorientation there would be a negative deviation of the experimental data from the volume-based prediction, because the complex would not persist as an entity for as long as τ_{OR} . In other words, the hydrodynamic volume would be represented by that of the chromophore and a fraction of the solvent volume, with the fraction being related to the ratio of the complex lifetime to τ_{OR} . Such an explanation is not without precedent. The formation of a persistent complex between chromophore and solvent has been invoked previously to explain state-dependent rotational diffusion behavior in oxazines in hydrogen-bonding solvents. 33-35

In an attempt to clarify this assertion, we acquired anisotropy decay data for **FR0**-HSB^{+*} in acidified methanol and ethanol solutions. Acidification of **FR0**-SB in methanol and ethanol produces **FR0**-HSB⁺, which has a characteristic absorption band centered at *ca*. 480 nm (Fig. S5). Direct excitation of this band yielded anisotropy decay time constants that are identical to those for **FR0**-HSB⁺ in the non-acidified solvents. We attribute this result to the limitations of the experiment. The addition of sufficient acid to produce **FR0**-HSB⁺ is practical only in methanol

and ethanol, and the hydrodynamic volumes of these solvents are small relative to the chromophore. Thus any difference between the reorientation of protonated **FR0**-HSB⁺ and the same chromophore interacting with the solvent is not resolvable within our experimental uncertainty.

A brief word is in order regarding the zero-time anisotropy decay data shown in Table 1. These data reflect the angle between the excited and emitting transition dipole moments. For **FR0**-SB* there appears to be a monotonic decline in $R(\theta)$ with increasing solvent viscosity while for **FR0**-HSB*+ $R(\theta)$ appears to be independent of solvent. For **FR0**-SB* the angle between the excited and emitting transition dipole moment varies between 15° and 49°, while for **FR0**-HSB*+ the angle is essentially constant at ~30°. The angle between the excited and emitting transition dipole moments depends on the structure of the emitting species and on the symmetries of the vibronic transitions accessed by the emission. As the details of solvation change with solvent, the specific vibronic transitions accessed over the detected emission window will vary.²⁸ While interesting, there simply is not enough information contained in $R(\theta)$ to be able to extract detailed chemical information.

We consider next the details of the proton exchange process. It is important to note at the outset that the primary factors mediating molecular rotation are different than those which mediate proton transfer. As noted above, the two emission bands shown in Fig. 2 correspond to **FR0**-SB* (*ca.* 460 nm) and **FR0**-HSB^{+*} (*ca.* 630 nm). We can explain the changes in the area of the two fluorescence emission bands in the context of a kinetic model, which can be evaluated using time-resolved measurements. The relative intensities of the two bands are expected to scale with the corresponding lifetimes of the unprotonated and protonated species in the different solvents, after considering differences in the fluorescence quantum yield between the unprotonated and

protonated species. Table 1 summarizes the fluorescence lifetime decays obtained from fitting the isotropic quantity $(I_{\parallel}(t) + 2I_{\perp}(t))$ to an exponential decay function. The lifetime data for **FR0**-HSB^{+*} (630 nm) exhibit two components, a rise time and a decay time. For the *n*-alcohols, we observe that all the lifetimes increase as a function of solvent aliphatic chain length. This dependence cannot be accounted for in terms of the solvent p K_a , which varies over a narrow range, from 15.5 to 17. Rather, the change in observed rates is seen to depend on the concentration of OH functionality in the solvents.

Table 1. Fluorescence anisotropy and lifetime components. All time constants are in ps. Uncertainties are reported as \pm 1 σ for at least three determinations. Abbreviations: MeOH = methanol, EtOH = ethanol, PrOH = 1-propanol, BuOH = 1-butanol, PeOH = 1-pentanol, HxOH = 1-hexanol, HpOH = 1-heptanol, OcOH = 1-octanol, EG = ethylene glycol.

Solvent	460 nm emission (SB*)				630 nm emission (HSB ⁺ *)			
	R(0)	τ_{OR} (ps)	$\tau_{\mathrm{SB1}}\left(\mathrm{ps}\right)$	$ au_{\mathrm{SB2}}\left(\mathrm{ps}\right)$	R(0)	$\tau_{\rm OR}$ (ps)	$\tau_{\rm X} ({\rm ps})$	$\tau_{\rm HSB}$ (ps)
MeOH	0.36 ± 0.01	86 ± 6	48 ± 4		0.24 ± 0.02	186 ± 13	96 ± 4	1048 ± 2
EtOH	0.31 ± 0.03	134 ± 16	74 ± 5	301 ± 24	0.24 ± 0.02	315 ± 8	208 ± 13	1262 ± 15
PrOH	0.23 ± 0.02	235 ± 23	94 ± 3	306 ± 6	0.25 ± 0.01	544 ± 17	296 ± 10	1443 ± 6
BuOH	0.19 ± 0.03	355 ± 19	213 ± 5	617 ± 31	0.25 ± 0.02	834 ± 8	426 ± 63	1585 ± 30
PeOH	0.14 ± 0.01	456 ± 29	361 ± 41	2201 ± 753	0.24 ± 0.01	1090 ± 49	610 ± 53	1604 ± 26
НхОН	0.10 ± 0.01	552 ± 43	437 ± 12	2824 ± 212	0.24 ± 0.01	1389 ± 32	739 ± 40	1663 ± 32
НрОН	0.06 ± 0.01	774 ± 17	605 ± 64		0.26 ± 0.01	1618 ± 22	773 ± 9	1774 ± 13
ОсОН	0.11 ± 0.01	931 ± 36	691 ± 72		0.25 ± 0.01	2020 ± 69	933 ± 17	1701 ± 55
EG	0.11 ± 0.05	2061 ± 76	57 ± 1	1328 ± 30	0.29 ± 0.06	3312 ± 146	100 ± 12	1133 ± 104

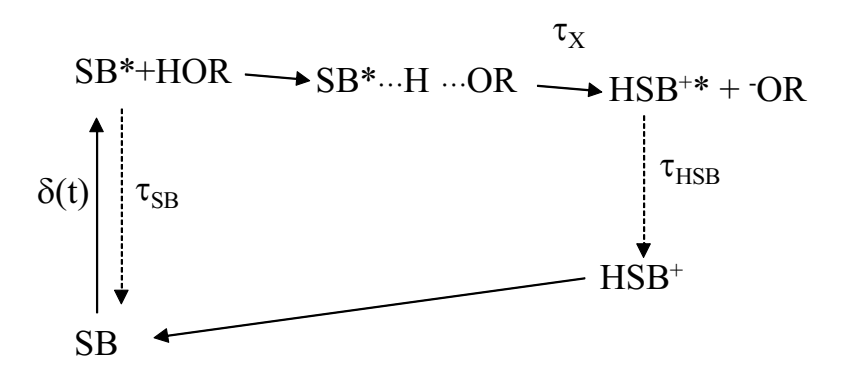


Fig. 5: Kinetic population model for excited state proton transfer between **FR0**-SB and the solvent.

A kinetic model, consistent with the steady-state emission data, is presented in Fig. 5. In this model, excitation ($\delta(t)$) is at 350 nm, producing FR0-SB*. This species can either relax radiatively to FR0-SB ($\tau_{\rm SB}$, $\lambda_{\rm em} \approx 460$ nm) or can interact with a solvent molecule through hydrogen bonding, leading to a transition state [FR0-SB*...H...OR]* and subsequent proton abstraction to produce FR0-HSB+* and $^{-}$ OR. Radiative relaxation of FR0-HSB+* ($\tau_{\rm HSB}$) is observed at ca. 630 nm. For the proton transfer process, we identify two different rate constants. The first rate constant is associated with hydrogen bonding between the solvent and FR0-SB*. We believe the formation of the H-bond to be fast. We assert that the risetime pertaining to the FR0-HSB+* population is associated with the formation of the complex (Fig. 4) and progression to the products, FR0-HSB+* + RO $^{-}$.

To assist the interpretation of the experimental data, we show in Table 2 some of the key properties of the low-lying singlet electronic states of the **FR0**-SB molecule obtained in the *ab* initio EOMCC calculations described in the Computational Details section. They include the excitation energies and oscillator strengths characterizing the vertical $S_0 \rightarrow S_n$ (n=1-4) transitions and the electronic dipole moments of the calculated ground and excited states. To verify

the reliability of our EOMCC-based computational protocol defined by Eq. (1), we compared our theoretical gas-phase value of the $S_0 \rightarrow S_1$ vertical excitation energy of **FR0**-SB with the corresponding experimental photoabsorption energy characterizing **FR0**-SB dissolved in hexane, which is the least polar solvent considered in our experiments that will be reported in a future publication. Our best *ab initio* EOMCC value based on Eq. (1), of 3.70 eV, matches closely the experimentally derived $S_0 \rightarrow S_1$ transition energy corresponding to the maximum of the photoabsorption band characterizing **FR0**-SB dissolved in hexane, which is 3.52 eV. If we did not correct the EOMCCSD/6-31+G* excitation energy for the triples using Eq. (1), we would obtain 4.10 eV, which shows that high-order many-electron correlation effects beyond the EOMCCSD level, estimated in this study with the help of the δ -CR-EOMCC(2,3) approach, are significant. We should also mention that our best TD-DFT result for the $S_0 \rightarrow S_1$ vertical excitation energy of **FR0**-SB, obtained using the CAMB3LYP functional, of 3.92 eV, is not as good as the EOMCC value shown in Table 2.

Table 2. The orbital character, vertical excitation energies $\omega_n^{(\text{EOMCC})}$, oscillator strengths, and electronic dipole moment values μ_n of the four lowest-energy excited singlet electronic states S_n of **FR0**-SB, as obtained in the EOMCC calculations described in the Computational Details section. The CCSD value of the dipole moment in the ground electronic state is 2.6 D.

State	Orbital	$\omega_n^{(\mathrm{EC}}$	OMCC)	Oscillator	μ_n (D)	
State	character	(eV)	(nm)	strength		
S_1	$\pi \to \pi^*$	3.70	335	0.74	8.6	
S_2	$\pi \to \pi^*$	3.96	313	0.35	6.7	
S_3	$\pi o \pi^*$	4.23	293	0.02	5.4	
S ₄	$\pi \to \pi^*$	4.45	279	0.03	4.3	

Moving to our main theoretical findings summarized in Table 2, we can see that of the four lowest-energy singlet excited states of **FR0**-SB calculated in the present study, two, namely, S_1 and S₂, can be accessed by photoabsorption. The remaining two states, S₃ and S₄, are characterized by negligible oscillator strengths. In a future computational study, we will show that the positions and relative intensities of the $S_0 \to S_1$ and $S_0 \to S_2$ transitions closely match those observed in high-resolution photoabsorption experiments for FR0-SB in nonpolar solvents, such as hexane. What is most important for the present study are the observations that both S₁ and S₂ have similar peak positions and intensities on the same order, resulting in broadening of the FR0-SB \rightarrow FR0-SB* photoabsorption band, and that the electronic dipole moment of FR0-SB increases significantly upon photoexcitation, from 2.6 D in the ground electronic state to 8.6 D for S₁ and to 6.7 D for S_2 . This more-or-less three-fold increase in the dipole moment as a result of the $S_0 \rightarrow$ S_1 and $S_0 \rightarrow S_2$ optical transitions in **FR0**-SB, observed in our EOMCC calculations and shown in Fig. 1b for S₁, demonstrates that the deprotonation of protic solvent molecules by the photoactivated FR0-SB species is indeed possible, since there is an accumulation of the net negative charge on the imine nitrogen. While the decay time constant corresponding to the second excited singlet state, τ_{SB2} , represents only a small fraction of the total population decay of FR0-SB*, and in some cases (methanol, n-heptane, and n-octane) this component cannot be even resolved, i.e., the S₂ state does not appear to play a direct role in proton exchange, the presence of this strongly dipolar state in the vicinity of S_1 , which has a similarly large dipole, may be important for understanding the state-dependent modulation of electron density in FR0-SB. In extracting the decay time constants τ_{SB1} and τ_{SB2} in Table 1, we made the assumption that the $S_1 \to S_0$ and $S_2 \to S_0$ fluorescence processes are independent of each other and that the radiative $S_2 \to S_1$ transition can be neglected, and our ab initio EOMCC calculations confirm the validity of these

assumptions. The oscillator strength characterizing the transition between the S_1 and S_2 states resulting from our calculations is only about 0.01, making the $S_2 \rightarrow S_1$ fluorescence highly unlikely. Gaining a detailed understanding of the role of each excited state in the optical response and proton transfer clearly requires more experimental investigation. We are presently investigating both the one- and two-photon excited emission data and will report on those data in a future publication.

The solvent-dependence of the fluorescence lifetimes is shown in Fig. 6 as a function of solvent viscosity (Fig. 6a) and as a function of the solvent [OH] (Fig. 6b). The dependence on [OH] is similar to the dependence on dielectric constant (not shown). The dependence of the radiative lifetimes of **FR0**-SB* and **FR0**-HSB^{+*} on viscosity indicates that relaxation for both is mediated by the ability of the chromophore to access out-of-plane conformations to activate non-radiative decay pathways. The dependence of τ_x on viscosity suggests that some level of solvent-solute alignment is required to facilitate the formation of the transition state.

Examining the lifetimes as a function of [-OH] reveals that all of the lifetimes are affected by the proton transfer process. For the highest proton concentrations (ethylene glycol and methanol) it appears that the formation of the transition state and the subsequent proton transfer event occurs on a timescale that is on the order of our experimental time resolution (ca. 40 ps) or faster. This result is expected based on the high concentration of -OH functionality that is present. The [-OH] dependence becomes more clear for solvents ethanol through n-octanol, where the concentration of [-OH] is lower. Such findings are consistent with the model shown in Fig. 5.

We note correlation between the population decay of **FR0**-SB* and build-up of **FR0**-HSB^{+*}. The time constant associated with the transition from **FR0**-SB* to **FR0**-HSB^{+*} (τ_X) is

longer in all cases than the decay time of **FR0-**SB*. These data demonstrate there is necessarily a transition state with a finite lifetime associated with the proton transfer process.

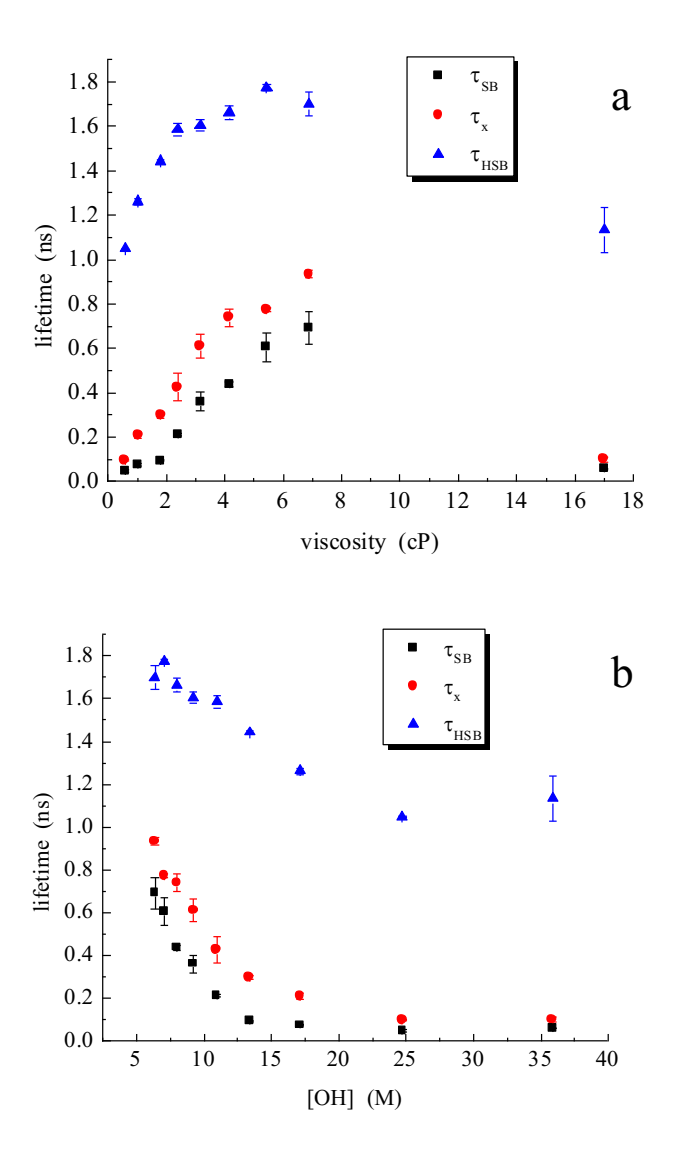


Fig. 6: (a) Dependence of lifetimes τ_{SB} , τ_{X} and τ_{HSB} on solvent viscosity. (b) Dependence of the same lifetimes on solvent [-OH].

Because the series of *n*-alcohols provide a correlation between solvent molecular structure and viscosity, with an inverse dependence on [-OH], it is important to test which of these properties dominates the several processes we consider in this paper. For the rotational diffusion data there

is a known viscosity dependence (Eq. (3)) and we observe this experimentally. For the lifetime data, ethylene glycol (furthest right points in Fig. 6a) does not follow the trend for the normal alcohols. As can be seen in Fig. 6b, however, the lifetime data exhibits a dependence on [-OH] that holds for both ethylene glycol and the n-alcohols, and such a finding is consistent with the kinetic model shown in Fig. 5.

It is also useful to consider the dependence of our lifetime data on the dielectric constant of the solvent. This dependence follows the same trend as shown in Fig. 6b for [-OH]. The dielectric constant is related to the ability of the environment to solvate charged species. The rise time of the protonated species τ_X decreases as the dielectric constant of the solvent increases. The stabilization of the solvent-solute complex as well as the formation of the charged species is mediated by the dielectric response of the system, which implies that both the transition state and the reaction products (**FR0**-HSB^{+*} and RO⁻) are more polar than the neutral **FR0**-SB* and ROH reactants. While this is obviously the case for the final products, the dependence of τ_X on dielectric constant sheds some light on the nature of the transition state.

It is also important to consider the dominant factor that mediates the relaxation of **FR0**-HSB^{+*}. As can be seen from the steady-state emission data (Fig. 2), the emission of **FR0**-HSB^{+*} shifts to the blue with increasing solvent aliphatic chain length, consistent with the polar (ionic) nature of the excited chromophore. Based on this observation one would expect on simple polarity grounds that the lifetime of **FR0**-HSB^{+*} would decrease with increasing solvent aliphatic chain length. Experimentally, the opposite trend is observed (Table 1). The lifetime of **FR0**-HSB^{+*} is seen to be proportional to [-O⁻], indicating that back-donation of the proton from **FR0**-HSB^{+*} to the alkoxide RO⁻ mediates the relaxation of the protonated chromophore. Consequently, the

species **FR0**-HSB⁺ shown in Fig. 5 may have a vanishingly small concentration, which is not surprising.

It is important to make a clear distinction between the rotational diffusion dynamics and the proton exchange dynamics seen here. Indeed, these two phenomena, which both play important roles in the data we report here, depend on the solvent properties in different ways. Specifically, the rotational diffusion dynamics are known to depend on the viscosity of the solvent system according to the modified DSE model. The proton exchange dynamics, in contrast, may depend on the solvent viscosity to a limited extent in the context of the time required to achieve intermolecular alignment to facilitate proton transfer and solvation dynamics. The dominant contributions to proton transfer dynamics, however, are the available -OH concentration and the solvent dielectric constant. The data for **FR0-SB*** and **FR0-HSB**** in ethylene glycol underscore the difference in the factors that dominate the two processes.

Conclusions

We have examined the rotational diffusion and excited state protonation/deprotonation dynamics of both **FR0**-SB* and **FR0**-HSB^{+*} species as a function of solvent viscosity and dielectric constant for a series of *n*-alcohols C1 (methanol) through C8 (*n*-octanol) and ethylene glycol. The rotational diffusion behavior of **FR0**-SB* and **FR0**-HSB^{+*} is seen to be substantially different and approximated by the modified DSE model in the slip and stick limits, respectively. It is the protonation of the **FR0**-SB* molecule that leads to a chromophore possessing formal charge and exhibiting substantially stronger solvent-solute interactions. We find better agreement when we consider that the solvent interacts with the excited chromophore over a timescale that is

similar to the chromophore rotational diffusion time. This finding provides strong evidence for the formation of a relatively stable transition state, as schematized in Fig. 4.

The lifetime of the excited states of both **FR0-SB*** and **FR0-HSB**** correlate with the [-OH] and the dielectric constant, which is consistent with the kinetic model presented in Fig. 5 and with the structure of the transition state being more polar than the neutral reactants. The dependence of each process on solvent parameters is different, and we expect that there are steric issues in addition to those we report here that can be revealed through the study of these processes in secondary and tertiary alcohols and in diols.

Taken collectively, these data demonstrate that the FR0-SB* super photobase extracts solvent protons efficiently and in a predictable manner. This is consistent with the significant, *ca.* three-fold, increase in the dipole moment upon photoexcitation to the two lowest-energy singlet excited states of FR0-SB observed in our high-level *ab initio* EOMCC calculations. While our decay time measurements suggest that the second excited singlet state, which has a large dipole moment similar to the first excited singlet state, does not play a direct role in proton exchange, its presence may be important for understanding the state-dependent modulation of electron density in FR0-SB. Our experiments reported in this work find the protonation step to be highly dependent on the ability of the solvent to solvate the resulting charged species. The use of photo-initiated reagents in precision chemistry applications can proceed with greater predictive power with the information gained from this work. In the future, we will explore other aspects of the complex interactions between FR0-SB* and its local environment to more fully understand the chemical and physical factors that mediate its photo-induced reactive properties.

Acknowledgments

GJB is grateful to the NIH for support of this work through grants 2R01EY016077-08A1 and 5R01EY025383-02 R01. This material is based upon work supported by the National Science Foundation (Grant No. CHE1836498 to MD) and the Chemical Sciences, Geosciences and Biosciences Division, Office of Basic Energy Sciences, Office of Science, U.S. Department of Energy (Grant No. DE-FG02-01ER15228 to PP). BB acknowledges the NIH for support of this project (R01GM101353).

References

- 1. Finkler, B.; Spies, C.; Vester, M.; Walte, F.; Omlor, K.; Riemann, I.; Zimmer, M.; Stracke, F.; Gerhards, M.; Jung, G., Highly Photostable "Super"-Photoacids for Ultrasensitive Fluorescence Spectroscopy. *Photochem. Photobiol. Sci.* **2014**, *13*, 548-562.
- 2. Malval, J.-P.; Diemer, V.; Savary, F. M.; Jacques, P.; Allonas, X.; Chaumeil, H.; Defoin, A.; Carré, C., Excited State Proton Transfer in a 'Super' Photoacid Based on a Phenol-Pyridinium Biaryl Chromophore. *Chem. Phys. Lett.* **2008**, *455*, 238-241.
- 3. Hunt, J. R.; Dawlaty, J. M., Photodriven Deprotonation of Alcohols by a Quinoline Photobase. *J. Phys. Chem. A* **2018**, *122*, 7931-7940.
- 4. Sheng, W.; Nairat, M.; Pawlaczyk, P. D.; Mroczka, E.; Farris, B.; Pines, E.; Geiger, J. H.; Borhan, B.; Dantus, M., Ultrafast Dynamics of a "Super" Photobase. *Angew. Chemie Int. Ed. Engl.* **2018,** *57*, 14742-14746.
- 5. Pillman, H. A.; Blanchard, G. J., Effects of Energy Dissipation on Motional Dynamics in Unilamellar Vesicles. *J. Phys. Chem. B* **2010**, *114*, 13703-13709.
- 6. Kohn, W.; Sham, L. J., Self-Consistent Equations Including Exchange and Correlation Effects. *Phys. Rev.* **1965**, *140*, A1133-A1138.
- 7. Hohenberg, P.; Kohn, W., Inhomogeneous Electron Gas. *Phys. Rev.* **1964,** *136*, B864-B871.
- 8. Čížek, J., On the Correlation Problem in Atomic and Molecular Systems. Calculation of Wavefunction Components in Ursell-Type Expansion Using Quantum-Field Theoretical Methods. *J. Chem. Phys.* **1966**, *45*, 4256-4266.

- 9. Stanton, J. F.; Bartlett, R. J., The Equation of Motion Coupled-Cluster Method. A Systematic Biorthogonal Approach to Molecular Excitation Energies, Transition Probabilities, and Excited State Properties. *J. Chem. Phys.* **1993**, *98*, 7029-7039.
- 10. Hehre, W. J.; Ditchfield, R.; Pople, J. A., Self-Consistent Molecular Orbital Methods. Xii. Further Extensions of Gaussian-Type Basis Sets for Use in Molecular Orbital Studies of Organic Molecules. *J. Chem. Phys.* **1972**, *56*, 2257-2261.
- 11. Hariharan, P. C.; Pople, J. A., The Influence of Polarization Functions on Molecular Orbital Hydrogenation Energies. *Theo. Chim. Acta* **1973**, *28*, 213-222.
- 12. Clark, T.; Chandrasekhar, J.; Spitznagel, G. W.; Schleyer, P. V. R., Efficient Diffuse Function-Augmented Basis Sets for Anion Calculations. Iii. The 3-21+G Basis Set for First-Row Elements, Li–F. *J. Comp. Chem.* **1983**, *4*, 294-301.
- 13. Fradelos, G.; Lutz, J. J.; Wesołowski, T. A.; Piecuch, P.; Włoch, M., Embedding Vs Supermolecular Strategies in Evaluating the Hydrogen-Bonding-Induced Shifts of Excitation Energies. *J. Chem. Theory Comp.* **2011**, *7*, 1647-1666.
- 14. Łoch, M. W.; Lodriguito, M. D.; Piecuch, P.; Gour, J. R., Two New Classes of Non-Iterative Coupled-Cluster Methods Derived from the Method of Moments of Coupled-Cluster Equations. *Mol. Phys.* **2006**, *104*, 2149-2172.
- 15. Erratum. Mol. Phys. **2006**, 104, 2991-2991.
- 16. Piecuch, P.; Gour, J. R.; Włoch, M., Left-Eigenstate Completely Renormalized Equation-of-Motion Coupled-Cluster Methods: Review of Key Concepts, Extension to Excited States of Open-Shell Systems, and Comparison with Electron-Attached and Ionized Approaches. *Int. J. Quant. Chem.* **2009**, *109*, 3268-3304.

- 17. Piecuch, P.; Włoch, M., Renormalized Coupled-Cluster Methods Exploiting Left Eigenstates of the Similarity-Transformed Hamiltonian. *J. Chem. Phys.* **2005**, *123*, 224105.
- 18. Piecuch, P.; Włoch, M.; Gour, J. R.; Kinal, A., Single-Reference, Size-Extensive, Non-Iterative Coupled-Cluster Approaches to Bond Breaking and Biradicals. *Chem. Phys. Lett.* **2006**, *418*, 467-474.
- 19. Purvis, G. D. I.; Bartlett, R. J., A Full Coupled-Cluster Singles and Doubles Model: The Inclusion of Disconnected Triples. *J. Chem. Phys.* **1982**, *76*, 1910-1918.
- 20. Piecuch, P.; Hansen, J. A.; Ajala, A. O., Benchmarking the Completely Renormalised Equation-of-Motion Coupled-Cluster Approaches for Vertical Excitation Energies. *Mol. Phys.* **2015**, *113*, 3085-3127.
- 21. Włoch, M.; Gour, J. R.; Kowalski, K.; Piecuch, P., Extension of Renormalized Coupled-Cluster Methods Including Triple Excitations to Excited Electronic States of Open-Shell Molecules. *J. Chem. Phys.* **2005**, *122*, 214107.
- 22. Yanai, T.; Tew, D. P.; Handy, N. C., A New Hybrid Exchange–Correlation Functional Using the Coulomb-Attenuating Method (Cam-B3lyp). *Chem. Phys. Lett.* **2004**, *393*, 51-57.
- 23. Casida, M. E., In *Recent Advances in Density Functional Methods, Part 1*, Chong, D. P., Ed. World Scientific: Singapore, 1995; pp 155-192.
- 24. Gordon, M. S.; Schmidt, M. W., In *Theory and Applications of Computational Chemistry:*The First Forty Years, Dykstra, C. E.; Frenking, G.; Kim, K. S.; Scuseria, G. E., Eds. Elsevier:

 Amsterdam, 2005; pp 1167-1189.
- 25. Piecuch, P.; Kucharski, S. A.; Kowalski, K.; Musiał, M., Efficient Computer Implementation of the Renormalized Coupled-Cluster Methods: The R-Ccsd[T], R-Ccsd(T), Cr-Ccsd[T], and Cr-Ccsd(T) Approaches. *Comp. Phys. Commun.* **2002**, *149*, 71-96.

- 26. Kowalski, K.; Piecuch, P., New Coupled-Cluster Methods with Singles, Doubles, and Noniterative Triples for High Accuracy Calculations of Excited Electronic States. *J. Chem. Phys.* **2004**, *120*, 1715-1738.
- 27. Humphrey, W.; Dalke, A.; Schulten, K., Vmd: Visual Molecular Dynamics. *J. Mol. Graph.* **1996,** *14*, 33-38.
- 28. Chuang, T. J.; Eisenthal, K. B., Theory of Fluorescence Depolarization by Anisotropic Rotational Diffusion. *J. Chem. Phys.* **1972**, *57*, 5094-5097.
- 29. Debye, P., *Polar Molecules* Chemical Catalog Co.: New York 1929; p 84.
- 30. Hu, C.-M.; Zwanzig, R., Rotational Friction Coefficients for Spheroids with the Slipping Boundary Condition. *J. Chem. Phys.* **1974**, *60*, 4354-4357.
- 31. Perrin, F., Mouvement Brownien D'un Ellipsoide I. Dispersion Diélectrique Pour Des Molécules Ellipsoidales. *J. Phys. Radium* **1934** *5*, 497-511.
- 32. Edward, J. T., Molecular Volumes and the Stokes-Einstein Equation. *J. Chem. Ed.* **1970**, 47, 261-270.
- 33. Blanchard, G. J., A Study of the State-Dependent Reorientation Dynamics of Oxazine 725 in Primary Normal Aliphatic Alcohols *J. Phys. Chem.* **1988**, *92*, 6303-6307.
- 34. Blanchard, G. J., Detection of a Transient Solvent-Solute Complex Using Time-Resolved Pump-Probe Spectroscopy. *Anal. Chem.* **1989**, *61*, 2394-2398.
- 35. Blanchard, G. J., Counterion-Dependent Reorientation Dynamics of an Oxazine in Polar Protic and Aprotic Solvents *J. Phys. Chem.* **1991**, *95*, 5293-5299.

TOC Graphic

